Neurobiology:

The Duplicated α7 Subunits Assemble and Form Functional Nicotinic Receptors with the Full-length α7

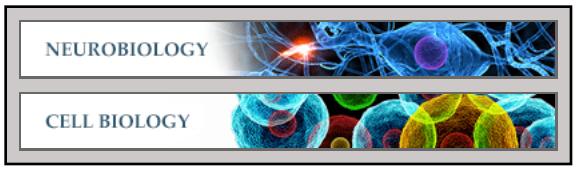

Ying Wang, Cheng Xiao, Tim Indersmitten, Robert Freedman, Sherry Leonard and Henry A. Lester

J. Biol. Chem. 2014, 289:26451-26463.
doi: 10.1074/jbc.M114.582858 originally published online July 23, 2014

THE JOURNAL OF BIOLOGICAL CHEMISTRY VOL. 289, NO. 38, pp. 26451–26463, Septemebr 19, 2014

The Duplicated α7 Subunits Assemble and Form Functional Nicotinic Receptors with the Full-length α7*

Received for publication, May 19, 2014, and in revised form, July 7, 2014 Published, JBC Papers in Press, July 23, 2014, DOI 10.1074/jbc.M114.582858

Ying Wang[‡], Cheng Xiao[‡], Tim Indersmitten[‡], Robert Freedman[§], Sherry Leonard[§], and Henry A. Lester[‡1]

From the [‡]Division of Biology and Biological Engineering, California Institute of Technology, Pasadena, California 91125 and the [§]Department of Psychiatry, University of Colorado at Denver, Denver, Colorado 80045

Background: Schizophrenia is linked to the α7 nicotinic acetylcholine receptor and to duplicated genes encoding truncated dupα7 and dupΔα7 subunits.
Results: Fluorescently labeled duplicated subunits display FRET with α7. Electrophysiology shows that duplicated subunits and α7 form heteropentamers with altered responses to choline and varenicline.
Conclusion: Duplicated subunits co-assemble with α7, forming functional receptors.
Significance: Such heteropentameric receptors could play a role in schizophrenia.

The α7 nicotinic acetylcholine receptor gene (*CHRNA7*) is linked to schizophrenia. A partial duplication of *CHRNA7* (*CHRFAM7A*) is found in humans on 15q13–14. Exon 6 of *CHRFAM7A* harbors a 2-bp deletion polymorphism, *CHRFAM7A-Δ2bp*, which is also associated with schizophrenia. To understand the effects of the duplicated subunits on α7 receptors, we fused α7, dupα7, and dupΔα7 subunits with various fluorescent proteins. The duplicated subunits co-localized with full-length α7 subunits in mouse neuroblastoma cells (Neuro2a) as well as rat hippocampal neurons. We investigated the interaction between the duplicated subunits and full-length α7 by measuring Förster resonance energy transfer using donor recovery after photobleaching and fluorescence lifetime imaging microscopy. The results revealed that the duplicated proteins co-assemble with α7. In electrophysiological studies, Leu at the 9′-position in the M2 membrane-spanning segment was replaced with Cys in dupα7 or dupΔα7, and constructs were co-transfected with full-length α7 in Neuro2a cells. Exposure to ethylammonium methanethiosulfonate inhibited acetylcholine-induced currents, showing that the assembled functional nicotinic acetylcholine receptors (nAChRs) included the duplicated subunit. Incorporation of dupα7 and dupΔα7 subunits modestly changes the sensitivity of receptors to choline and varenicline. Thus, the duplicated proteins are assembled and transported to the cell membrane together with full-length α7 subunits and alter the function of the nAChRs. The characterization of dupα7 and dupΔα7 as well as their influence on α7 nAChRs may help explain the pathophysiology of schizophrenia and may suggest therapeutic strategies.

Schizophrenia is a complex neuropsychiatric disorder. Its heterogeneity, incomplete penetrance, and environmental factors provide challenges for identifying genetic defects. On-line Mendelian Inheritance in Man now lists more than 200 candidate genes for schizophrenia susceptibility. Many genes have been associated with schizophrenia, yet there is no definitive genetic model. The etiology may involve a set of genes predisposing to the illness (1, 2).

One of the replicated candidate genes for schizophrenia is the α7 nicotinic acetylcholine receptor (nAChR)[2] subunit gene, *CHRNA7*. Both pharmacological and genetic studies support a potential link between the α7 nAChR and the pathophysiology of schizophrenia. The expression of the α7 receptor, as measured by α-bungarotoxin binding, is decreased in postmortem hippocampus, cortex, and thalamus of schizophrenic subjects (3–6). Moreover, *CHRNA7* localized at 15q14 is linked to the P50 auditory sensory processing deficit in schizophrenia by genetic and neurobiological studies (7, 8). Polymorphisms in the 5′ upstream regulatory region and intron 2 of *CHRNA7* are associated with both schizophrenia and the sensory processing deficit (9, 10).

The human *CHRNA7* gene is partially duplicated. Exons 5–10 of *CHRNA7* and additional DNA (~200 kbp) were duplicated upstream, interrupting a second partial duplication of four exons from the gene *ULK4* on chromosome 3 (11, 12). This duplication appears to be a relatively recent event unique to humans (13). The partially duplicated chimeric gene, *CHRFAM7A*, is located at 15q14 1.6 Mb centromeric to the full-length gene, and it is almost always in the opposite orientation to *CHRNA7*. In this duplication, exons 5–10, intervening introns, and the 3′-untranslated region of *CHRNA7* are conserved. The gene product, dupα7, lacks the signal peptide and part of the binding site but contains all of the α7 membrane-spanning regions. Mutation screening in human DNA and mRNA identified a 2-bp deletion polymorphism in exon 6 of *CHRFAM7A* (14). The partial duplication with the 2-bp deletion, *CHRFAM7AΔ2bp*, is almost always in the same orienta-

* This work was supported, in whole or in part, by National Institutes of Health Grant MH088550.
[1] To whom correspondence should be addressed: Division of Biology and Biological Engineering, California Institute of Technology, Pasadena, CA 91125. Tel.: 626-395-4946; Fax: 626-564-8709; E-mail: lester@caltech.edu.

[2] The abbreviations used are: nAChR, nicotinic acetylcholine receptor; dupα7, partial duplication of human α7; dupΔα7, partial duplication of human α7 with 2-bp deletion in exon 6; DRAP, donor recovery after photobleaching; FLIM, fluorescence lifetime imaging microscopy; SCAM, substituted cysteine accessibility method; MTSEA, ethylammonium methanethiosulfonate; ACh, acetylcholine; MTS, methanethiosulfonate; FP, fluorescent protein; GAT1, GABA transporter subtype 1.

tion as *CHRNA7* (15). The 2-bp deletion in exon 6 causes a frameshift in translation, resulting in a smaller gene product, dupΔα7, which lacks nearly the entire ligand-binding site compared with dupα7. *CHRFAM7AΔ2bp* is significantly associated with schizophrenia (16, 17), suggesting that the duplicated gene might contribute to cognitive impairment.

The gene products of *CHRFAM7A*, both mRNA and protein, are found in brain and also in the periphery (11). When expressed alone in cell lines or *Xenopus* oocytes heterologously, the protein product of *CHRFAM7A*, dupα7, is detected at low levels, but no functional receptor is observed (18). When either dupα7 or dupΔα7, the protein product of *CHRFAM7AΔ2bp*, is co-expressed with α7 in *Xenopus* oocytes, it reduces the amplitude of the acetylcholine (ACh)-evoked currents, and two previous studies show that the reduction increases with the dose of dupα7 (19, 20). The pharmacology of the expressed receptors shows differences from that of the α7 heteromer (20). Immunological studies in GH4C1 cells show that dupα7 reaches the plasma membrane (20). The authors of these previous studies suggest that *CHRFAM7A* acts as a dominant negative modulator of *CHRNA7* function in humans and thus may be critical for receptor regulation (19, 20).

This study further characterizes the role of *CHRFAM7A* by investigating how dupα7 and dupΔα7 exert their effects on the full-length α7 nAChR. We have studied the interaction between fluorescently labeled duplicated and full-length subunits in mouse neuroblastoma cells (Neuro2a) using imaging techniques. We concentrated on the possible stoichiometry of the assembled complexes. We have also performed electrophysiology recordings to examine the receptor properties. We confirm that the duplicated subunits are assembled and transported to the cell membrane together with full-length α7 and thus alter the function of the nAChRs. Our results contribute to the understanding of the pathophysiology of schizophrenia and suggest therapeutic strategies.

EXPERIMENTAL PROCEDURES

Reagents—Unless otherwise indicated, all chemicals for culture were purchased from Invitrogen, and all chemicals for electrophysiology were purchased from Sigma.

Plasmid Constructs—Human α7, dupα7, and dupΔα7 cDNA clones in pcDNA 3.1 were described previously (19). The fluorescent protein (FP) cassette, containing an Ala-Gly-Ala linker flanking the FP open reading frame on both sides, was fused into the M3-M4 loop of the subunits (21). The fusion site was chosen as described previously (22). Mutations were introduced using the QuikChange kit from Stratagene (La Jolla, CA) according to the manufacturer's instructions.

Cell Culture and Transfections—Mouse Neuro2a cells obtained from American Type Culture Collection (ATCC) were maintained in 45% Dulbecco's modified Eagle's medium (DMEM), 45% Opti-MEM, 10% fetal bovine serum (FBS) and supplemented with penicillin and streptomycin. Neuro2a cells were transfected with BioT (Bioland Scientific LLC, Paramount, CA) according to the manufacturer's instructions. Plasmid concentrations used for transfection were as follows: for imaging, 1 μg of each fluorescently labeled nAChR subunit; for competition experiments, 500 ng of each fluorescently labeled subunit + 1 μg of untagged subunit; for recording, 1 μg of each fluorescently labeled nAChR subunit + 200 ng of RIC-3. Rat hippocampal neurons were dissociated from day 18 rat embryos and plated on 35-mm glass-bottomed imaging dishes (MatTek, Ashland, MA) as described previously (23). Neurons were transfected after 7 days in culture using Lipofectamine 2000 in conjunction with Nupherin (Biomol Research Laboratories, Plymouth Meeting, PA) according to the manufacturer's instructions (24). 1 μg of each fluorescently labeled subunit was used.

Confocal Imaging—Neuro2a cells were plated at 90,000 cells per dish and imaged live 48 h after transfection. Before imaging, cell culture medium was replaced with phenol red-free CO_2-independent Leibovitz L-15 medium. Cells were imaged with a Nikon (Nikon Instruments, Melville, NY) C1 laser-scanning confocal microscope system equipped with a 63 × 1.4 numerical aperture VC Plan Apo oil objective. Pinhole diameter was 30–60 μm, and cells were imaged at 12-bit intensity resolution over 512 × 512 pixels at a pixel dwell time of 6.12 μs. Cellular mGFP and mCherry fluorescent signals were acquired by simultaneous excitation with 488-nm (for mGFP) and 561-nm (for mCherry) lasers. Emission spectra were acquired in 5-nm bins between 500 and 660 nm, and the signal of each expressed fluorophore was linearly unmixed from the raw spectral image using reference spectra from control cells expressing only mGFP or only mCherry fusion constructs. For each pixel of a spectral image, intensity of mGFP and mCherry was determined from fluorescence intensity values at the peak emission wavelength derived from the reference spectra.

Förster Resonance Energy Transfer (FRET) by Donor Recovery after Acceptor Photobleaching (DRAP)—To examine FRET between nAChR subunits, the acceptor photobleaching method (21) was used with a modified DRAP macro built into the EZC1 imaging software (Nikon). The fluorescence intensity of mGFP and mCherry was recorded simultaneously using a 488- and 561-nm laser, respectively, during a six-step incremental photodestruction of mCherry with a 561-nm laser and normalized to the prebleach time point. I_D value was extrapolated from a scatterplot of the fractional increase of mGFP *versus* the fractional decrease of mCherry. FRET efficiency was calculated as $E = 1 - (I_{DA}/I_D)$, where I_{DA} represents the normalized fluorescence intensity of mGFP (100%) in the presence of both donor (mGFP) and acceptor (mCherry), and I_D represents the normalized fluorescence intensity of mGFP in the presence of donor only (complete photobleaching of mCherry). Data were averaged from 20 to 30 cells per condition and reported as mean ± S.E.

FRET measurements may include contributions from pairs of fluorophores that are nearby but not in a macromolecular complex. In the biophysical literature, this has also been termed stochastic FRET, bystander FRET, background FRET, and proximity FRET. King *et al.* (25) calculated and measured that proximity FRET became negligible for tetramers at membrane densities less than $\sim 10^{-3}$ receptors/nm^2 or 10^3 receptors/μm^2, and similar estimates would apply to pentamers. The closely packed acetylcholine receptors at the nerve-muscle synapse have densities of 10^4/μm^2. For this study, densities on the plasma membrane were probably $<10^2$/μm^2, judging by the

small size of the currents we observed, by the fact that receptors were not evident in membrane profiles, and by the fact that we have rarely observed signals from single α7 nAChRs in membrane patches studied by zero-mode waveguides (26); measurements from Simonson *et al.* (27) yielded a similar conclusion. A more substantial, but less measurable, source of stochastic FRET would arise from fluorophores in the endoplasmic reticulum membrane. Total internal reflection fluorescent measurements of endoplasmic reticulum-resident heteromeric nAChRs (28) have led us to the assumption that these densities are $<10^3/\mu m^2$; and the much lower signals observed in this study led us to an estimate of $<10^2/\mu m^2$ in the endoplasmic reticulum. Thus, we conclude that proximity FRET has played little or no role in our measurements. An abundance of caution leads us to assume that in DRAP mode, FRET efficiencies of <10% may include a contribution from proximity FRET.

FRET by Fluorescence Lifetime Imaging Microscopy (FLIM)—We have monitored the fluorescence lifetime τ by time-correlated single-photon counting. YFP (donor)- and mCherry (acceptor)-tagged nAChRs were co-expressed in Neuro2a cells. We excited YFP with a picosecond pulsed laser (514 nm) and monitored the fluorescence emission using a time-correlated single-photon counting module (PicoQuant, West Springfield, MA). Data were collected at 530 ± 20 nm through a bandpass filter. Laser power was adjusted to give average photon-counting rates of the order 10^4 to 10^5 photons/s to avoid pulse pile up. The decay of the YFP fluorescent intensity was fitted into either a single exponential (when YFP is present alone) or a double exponential (when YFP and mCherry are present) with SymPhoTime software (PicoQuant) using Equation 1,

$$I(t) = A_1 e^{-t/\tau_1} + A_2 e^{-t/\tau_2} \quad \text{(Eq. 1)}$$

where τ_1 is the fluorescence lifetime of a YFP molecule when it is present alone, and τ_2 is the fluorescence lifetime of a YFP molecule when it interacts with its acceptor mCherry. We calculated the "binding fraction" and FRET efficiency using Equations 2 and 3,

$$P_{FRET} = \frac{A_2}{A_1 + A_2} \quad \text{(Eq. 2)}$$

$$E_{FRET} = 1 - \frac{\tau_2}{\tau_1} \quad \text{(Eq. 3)}$$

where P_{FRET} is the binding fraction, the fraction of YFP molecules that interact with mCherry, and E_{FRET} is the FRET efficiency.

Whole-cell Patch Clamp Recordings—Neuro2a cells were plated on 12-mm glass coverslips within 35-mm plastic bottom cell culture dishes at the density of 50,000 cells per dish. 48–72 h after transfection, glass coverslips were transferred to the recording chamber on the microscope stage. Expressing cells were identified and visualized as follows. Green (mGFP) and red (mCherry) fluorescence was visualized with an upright microscope (BX50WI, Olympus) and UV illumination with appropriate excitation filters. Cells were voltage-clamped at a holding potential of −65 mV. Agonists were applied using a focal drug application system to minimize desensitization (29). For concentration-response studies, ACh was applied from the lowest to highest concentration at 3-min intervals to get the dose-response curve. Whole-cell patch clamp recordings were performed with a MultiClamp 700B amplifier, a 1322 analog-to-digital converter, and pCLAMP 9.2 software (all from Axon Instruments, Molecular Devices). Data were sampled at 10 kHz and filtered at 2 kHz.

The intrapipette solution contained (in mM) the following: 135 potassium gluconate, 5 KCl, 5 EGTA, 0.5 $CaCl_2$, 10 HEPES, 2 Mg-ATP, and 0.1 GTP; the pH was adjusted to 7.2 with Tris base and the osmolarity to 300 mOsM with sucrose. The extracellular solution contained (in mM) the following: 140 NaCl, 5 KCl, 2 $CaCl_2$, 1 $MgCl_2$, 10 HEPES, and 10 glucose; pH was adjusted to 7.3 with Tris base. The Nernst potential for Cl^- in the intrapipette solution is −82.9 mV. The bath was continuously perfused with extracellular solution at room temperature. The patch electrodes had resistances of 5–8 megohms. The junction potential between the patch pipette and the bath solutions was nulled just before forming a seal. Series resistance was monitored and compensated by 70–80% throughout the recordings. The data were ignored if the series resistance (15–30 megohms) changed by >20% during the recording session.

For the substituted cysteine accessibility method (SCAM), each cell received one initial baseline application of ACh (300 μM), one control ACh application, an application of ethylammonium methanethiosulfonate (MTSEA, 2 mM, Toronto Research Chemicals Inc., North York, ON, Canada), and then a follow-up experimental application of ACh. The peak amplitude of control responses and experimental responses were calculated relative to baseline ACh responses to normalize the data.

RESULTS

Co-localization of Fluorescently Labeled dupα7/dupΔα7 Subunits and the Full-length α7—Based on previous work (21, 22), we fused fluorescent protein to the M3-M4 loop of full-length human α7 nAChRs as well as the dupα7 and dupΔα7 subunits (Fig. 1*A*). Fluorescently labeled subunits are co-expressed in Neuro2a cells and imaged alive using a confocal microscope (Fig. 1*B*). We noted that the heterologous expression of duplicated subunits was low. The chimeric gene, *CHRFAM7A,* is transcribed efficiently, but translation is poor (19). The intensity of the FP attached to these subunits was ~5% of the intensity of the FP attached to the full-length subunits. When co-expressed with fluorescent α7, the duplicated subunits were localized primarily in the endoplasmic reticulum, similar to the localization of the full-length receptors. We did not systematically study localization at the plasma membrane. The merged images of the GFP and mCherry signals indicate that both dupα7 and dupΔα7 subunits co-localize with the full-length α7 receptor very well. Pearson correlation coefficients were as follows: α7GFP with dupα7mCherry, 0.96 (n = 26); α7GFP with dupΔα7mCherry, 0.95 (n = 25); dupα7GFP with α7mCherry, 0.96 (n = 27); and dupΔα7GFP with α7mCherry, 0.97 (n = 26). We then co-expressed the duplicated and the full-length subunits in primary rat hippocampal neurons. Because of the low intensity of the labeled duplicated

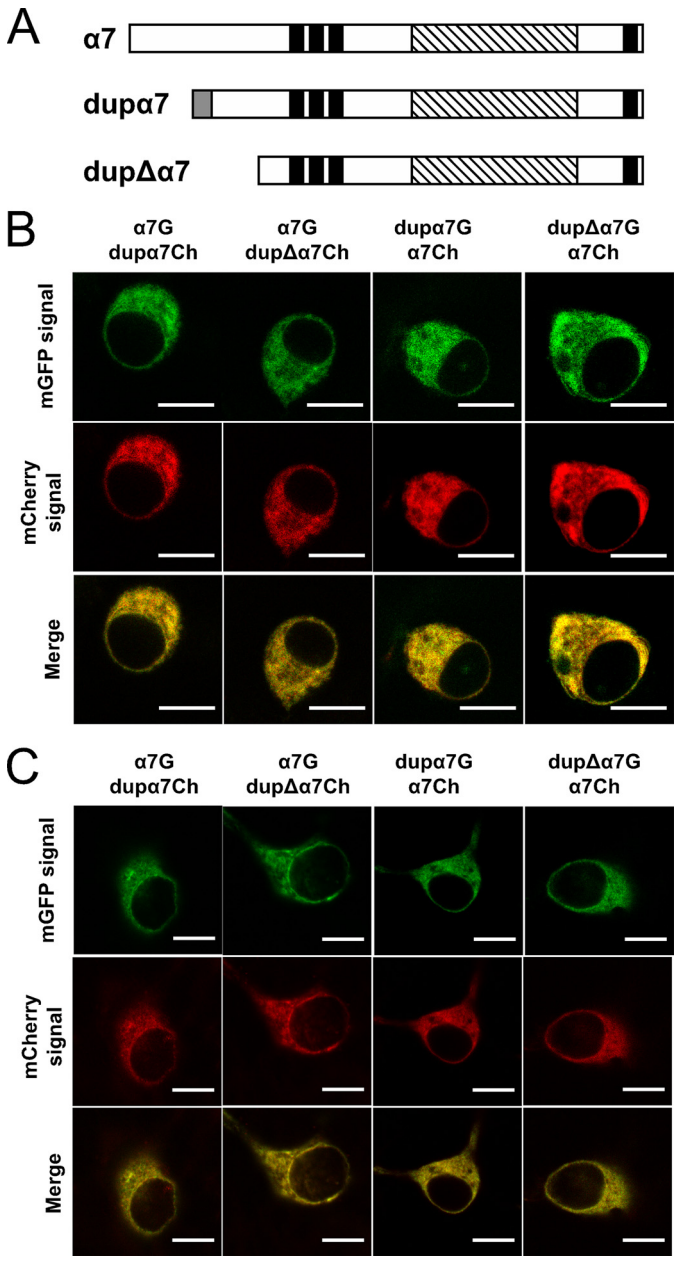

FIGURE 1. **Co-localization of fluorescently labeled duplicated subunits with full-length α7 in representative confocal cross-sections.** *A,* schematics of fluorescently labeled constructs. *α7* is full-length human α7 nAChR; *dupα7* is partial duplication of human α7; *dupΔα7* is partial duplication of human α7 with a 2-bp deletion. *Black boxes* represent transmembrane domains; *gray box* represents duplication of sequences from gene *ULK4* on chromosome 3, and *striped boxes* represent fluorescent proteins fused into the M3-M4 loop of nAChRs. *B,* duplicated subunits and full-length α7 receptors are localized similarly in Neuro2a cells. Neuro2a cells were transfected with the indicated nAChR cDNAs and were imaged live with spectral confocal microscopy 48 h after transfection. Spectral images were acquired, and specific mGFP and mCherry signals were extracted with linear unmixing. Fluorophore abbreviations are as follows: *G,* mGFP; *Ch,* mCherry. *Green* (*mGFP signal*) and *red* (*mCherry signal*) pseudocolor was assigned, and *yellow* (*Merge*) indicates co-localized proteins. *C,* duplicated subunits and full-length α7 receptors are localized similarly in the cell soma in primary neurons. E18 rat hippocampal neurons were plated and cultured for 14 days followed by transfection with the indicated nAChR cDNAs. One day after transfection, cells were imaged live using confocal microscopy. Normalization was done to emphasize co-localization and differed for the full-length *versus* duplicated constructs. Without normalization, the merged signal is mostly *green* (when α7mGFP is expressed) or *red* (when α7mCherry is expressed) and provides little information about co-localization. All images in *C* are less bright than *B* because the overall protein expression level is lower in primary neurons (*C*) than in Neuro2a cells (*B*). *Scale bar,* 10 μm.

subunits, they were not detected in the distal sites such as axons and dendrites. In the cell soma, where we were able to detect the duplicated subunits, both dupα7 and dupΔα7 were co-localized with the full-length α7 (Fig. 1*C*). Pearson correlation coefficients were as follows: α7GFP with dupα7mCherry, 0.85 (n = 11); α7GFP with dupΔα7mCherry, 0.86 (n = 11); dupα7GFP with α7mCherry, 0.93 (n = 10); and dupΔα7GFP with α7mCherry, 0.91 (n = 12).

Interaction between dupα7/dupΔα7 Subunits and the Full-length α7, DRAP Assays—The fact that the duplicated and the full-length subunits are co-localized both in Neuro2a cells and in the cell body of neurons suggests that they may be assembled into oligomers. The receptor assembly of nicotinic subunits is often measured by immunoprecipitation (30). This approach has limited applicability, however, for dupα7 and dupΔα7, due both to the extremely low protein levels and the lack of immune reagents selective for the duplicated subunits.

To directly determine whether the duplicated subunits interact with the full-length α7, we measured FRET between fluorescently tagged receptor subunits. FRET occurs only when donors and acceptors are within ~100 Å. When the fluorescent proteins are fused into the M3-M4 loop of nicotinic receptor subunits, subunits within pentamers undergo FRET. We have previously developed experimental approaches, well supported by theory, to analyze the assembly and subunit stoichiometry of such subunits within Cys loop receptors (23, 28, 31–33). For the present experiments, important guidelines arise from the strong distance dependence of FRET. Thus, for DRAP experiments adjacent subunits have considerably higher FRET values than nonadjacent subunits, and a donor adjacent to two acceptors displays higher FRET than one adjacent to zero or one acceptor.

We first employed DRAP to measure FRET between subunits (34). An mGFP/mCherry FRET pair was used for good separation of the excitation and emission spectra. We incrementally bleached mCherry at 561 nm while monitoring fluorescence intensity of both mGFP and mCherry, at 488 and 561 nm, respectively. Changes in fluorescence intensity *versus* time were plotted for each cell, and FRET efficiency was calculated as described under "Experimental Procedures." DRAP data revealed several types of co-assembly as follows: α7 with α7; α7 with dupα7; α7 with dupΔα7; dupα7 with dupα7; and dupΔα7 with dupΔα7 (Fig. 2*A*). The measured FRET efficiencies were different between reciprocal pairs. FRET efficiency was greater when dupα7, or dupΔα7, was the donor. This is likely due to the low expression of the duplicated gene; a dupα7 subunit is more likely to lie adjacent to an α7 subunit in the heteromeric receptor.

To confirm the interaction between the duplicated subunits and the full-length subunit, we measured FRET between α7-mGFP and α7-mCherry when untagged competing subunits were co-expressed. Calculated FRET efficiency showed that co-expression of untagged subunits, either duplicated or full-length, significantly decreased the FRET efficiency of the α7-mGFP/α7-mCherry pair (Fig. 2*B*), suggesting the specific interaction between dupα7/dupΔα7 subunits and the full-length α7.

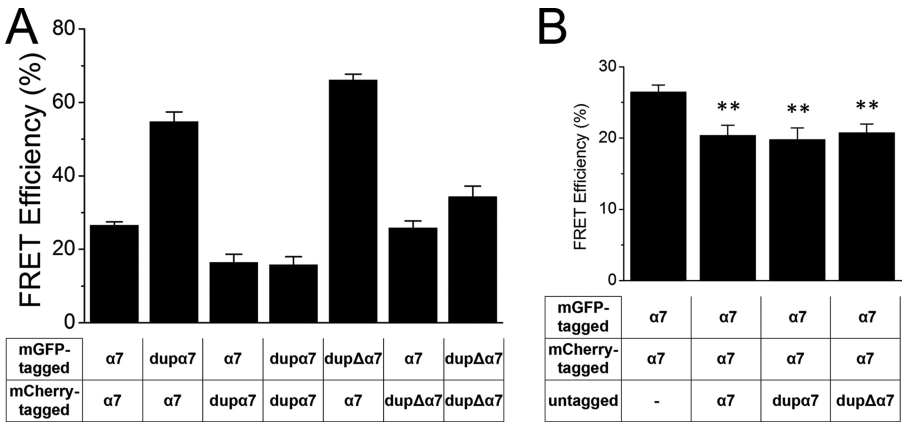

FIGURE 2. **DRAP revealed assembly of duplicated subunits with full-length α7.** *A,* FRET efficiency was measured by DRAP in Neuro2a cells. Several types of co-assembly were detected as follows: α7 with α7; α7 with dupα7; α7 with dupΔα7; dupα7 with dupα7; and dupΔα7 with dupΔα7. *B,* co-expression of untagged competing subunits decreased the FRET efficiency of the α7-mGFP/α7-mCherry pair. *Error bars* are ± S.E., and $n = 20–30$ cells for each condition. **, $p < 0.01$ compared with first condition.

Potential Stoichiometry of α7dupα7 and α7dupΔα7 Heteromers, FLIM Measurements—DRAP is not optimal for determining subunit stoichiometry in the present experiments because there are many more full-length α7 subunits than duplicated subunits when they are co-expressed (32). We also employed FLIM to measure FRET. The fluorescence decay profile of the donor, YFP molecules, was acquired from the entire cell with the use of a time- and space-correlated single-photon counting detector and was fitted to a double exponential time course (Fig. 3*A*). Neuro2a cells transfected with various nAChR cDNAs were monitored alive. The binding fraction, the fraction of donor that interacts with the acceptor, and FRET efficiency were calculated as described under "Experimental Procedures." In the context of analyses presented elsewhere, we believe that the binding fraction is best interpreted as the fraction of donors adjacent to one or more acceptors (23, 28, 31, 32). These two metrics are relatively insensitive to fluorophore concentration and light-path length, conditions that are poorly controlled inside a cell (35, 36). FLIM data confirmed several types of co-assembly as follows: α7 with α7; α7 with dupα7; α7 with dupΔα7; dupα7 with dupα7; and dupΔα7 with dupΔα7 (Fig. 3*B*).

To investigate the stoichiometry of α7/dupα7 and α7/dupΔα7 heteromers, we measured FRET between various pairs when untagged competing subunits were co-expressed. Both binding fraction and FRET efficiency of the α7-YFP/α7-mCherry pair were decreased, as expected, by untagged full-length α7 (Fig. 3, C_1 and C_2). Interestingly, co-expression of untagged duplicated α7 decreased binding fraction but not FRET efficiency of the α7-YFP/α7-mCherry pair, suggesting a limited incorporation of the duplicated subunits. In an $(\alpha7\text{-YFP})_1(\alpha7\text{-mCherry})_4$ configuration, as the number of untagged full-length subunits increases, the donor is less likely to be adjacent to an acceptor, which results in a decrease in the binding fraction. In contrast, if only one acceptor can be replaced by the duplicated subunit, the donor is still adjacent to an acceptor; thus one expects only a modest change in the binding fraction, and this is observed experimentally (Fig. 3C_1). Furthermore, when untagged full-length α7 was co-expressed for competition, both binding fraction and FRET efficiency of dupα7-YFP/α7-mCherry and dupΔα7-YFP/α7-mCherry pairs were decreased significantly. The difference between the reciprocal conditions, dupα7 competing for α7-YFP/α7-mCherry pair and α7 competing for dupα7-YFP/α7-mCherry pair, also supports the limited incorporation of duplicated subunits; more than one acceptor can be replaced by untagged subunits when α7 is competing, decreasing FRET substantially.

FRET Shows Assembly of dupα7 and dupΔα7 Subunits with Other Nicotinic Acetylcholine Subunits—We examined whether the duplicated subunits interact with other nicotinic receptor subunits. We co-expressed α4-mCherry or α3-mCherry subunits with YFP-tagged α7 subunits, either duplicated or full-length, in Neuro2a cells and measured FRET using FLIM (Fig. 4). Extensive quantitative analysis is not possible because of two complicating factors (32). 1) The α4, α3, and α7 subunits differ substantially in the size of their M3-M4 regions. 2) The fluorescent proteins may be inserted at differing orientations within these nonhomologous loops. Nonetheless, the results showed that both duplicated and full-length α7 interacted with α4 subunits (Fig. 4, A_1 and A_2). The FRET efficiency of a reciprocal pair, α4-YFP/α7-mCherry, was comparable with that of the α7-YFP/α4-mCherry pair, but the binding fraction is lower, probably due to larger numbers of α4-YFP subunits in the cells. The FRET efficiency of dupα7-YFP/α4-mCherry was higher than that of the α7-YFP/α4-mCherry pair, suggesting that α7 subunits, both duplicated and full-length, assembled with α4 into trimers or higher order multimers. If α7-YFP and dupα7-YFP only form dimers with α4-mCherry, the FRET efficiency will be the same for α7-YFP/α4-mCherry and dupα7-YFP/α4-mCherry.

To confirm the specificity of the interaction detected by FLIM, we co-expressed untagged competing α4 subunits with the α7-YFP/α7-mCherry pair; both binding fraction and FRET efficiency were decreased (Fig. 4, C_1 and C_2). In contrast, co-expression of untagged GABA transporter GAT1 (31) had no effect on the α7-YFP/α7-mCherry pair. When untagged α7 was used for competition, binding fraction but not FRET efficiency of the α7-YFP/α4-mCherry pair was decreased, whereas both binding fraction and FRET efficiency of dupα7-YFP/α4-mCherry and dupΔα7-YFP/α4-mCherry pairs were affected (Fig. 4, D_1 and D_2). Furthermore, both full-length and dupli-

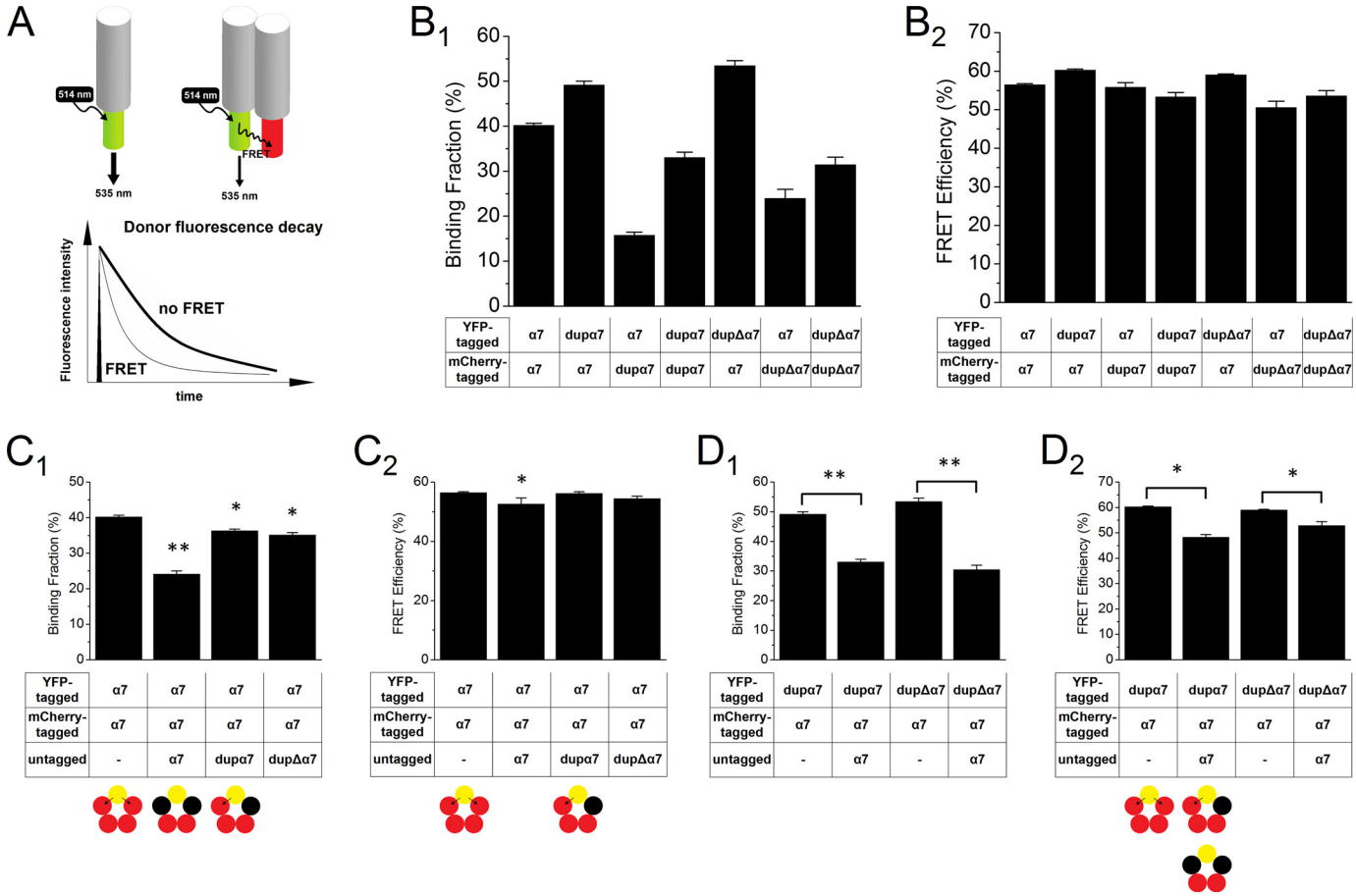

FIGURE 3. **FLIM confirmed assembly of duplicated subunits with full-length α7.** *A,* schematic of FRET occurring when a donor, the YFP (*yellow-green cylinder*) molecule attached to a nAChR subunit (*gray cylinder*), and an acceptor, the mCherry (*red cylinder*) molecule attached to a nAChR subunit, are in close proximity, usually <10 nm. The nonradiative transfer of excited state energy of the donor to the acceptor shortens the donor fluorescence lifetime and results in a faster decay in the fluorescence intensity of the donors. B_1 and B_2, Neuro2a cells were transfected with the indicated nAChR subunits and were imaged alive using FLIM. Binding fraction (B_1) and FRET efficiency (B_2) were calculated as described under "Experimental Procedures." Several types of co-assembly were detected as follows: α7 with α7, α7 with dupα7, α7 with dupΔα7, dupα7 with dupα7, and dupΔα7 with dupΔα7. C_1 and C_2, additional expression of untagged competing subunits (*black circles*) decreased the binding fraction of the α7-YFP/α7-mCherry pair. **, $p < 0.01$; *, $p < 0.05$ *versus* first condition. D_1 and D_2, additional expression of untagged full-length α7 subunit decreased both binding fraction and FRET efficiency of the dupα7-YFP/α7-mCherry and dupΔα7-YFP/α7-mCherry pairs. *Error bars* are ± S.E., and $n = 20–30$ cells for each condition. **, $p < 0.01$; *, $p < 0.05$.

cated α7 display robust FRET with α3 nAChR subunits (Fig. 4, E_1 and E_2).

dupα7 and dupΔα7 Subunits Form Functional Receptors with α7 Subunits—The SCAM is appropriate to identify the residues lining the lumen of ion channels (37, 38). The cysteine sulfhydryl forms a disulfide bond with sulfhydryl-specific reagents, methanethiosulfonate (MTS) derivatives, including MTS-ethylammonium (MTSEA), ethyltrimethylammonium, and ethylsulfonate. A cysteine mutation is generated to replace a particular residue; if this residue lies in the lumen of the ion channel and is accessible from the extracellular solution, MTS derivatives alkylate the cysteine and alter ion channel function.

Leucine at the 247-position of α7 nicotinic receptors resides ~9 residues downstream from the cytoplasmic beginning of the M2 pore-lining region (termed the 9′-position in most studies, because the M2 domain is rather well conserved among Cys loop receptors). The M2 domain of dupα7 and dupΔα7 has the same sequence as α7 in this domain. We replaced the Leu-9′ residue with cysteine (L9′C mutation) in dupα7 and dupΔα7. We transfected these subunits individually with α7 subunits and measured receptor function with the whole-cell patch clamp technique. If dupα7 and dupΔα7 subunits assemble with α7 subunits to form functional receptors, we expect the introduced cysteines in dupα7 and dupΔα7 to be accessible for MTSEA and MTSEA to change receptor function. As the α7 subunit has a cysteine at the 116-position, to eliminate the possibility that MTS derivatives bind to the endogenous cysteine and distort the results, we replaced this cysteine with serine in all of the constructs. The aligning mutation in dupα7 and dupΔα7 has different numbers but are termed C116S for consistency. Previous reports show that the C116S does not alter α7 receptor function (39).

Using the whole-cell patch clamp technique and a focal drug application system (29, 40), we examined 300 μM ACh-evoked inward current (I_{ACh}) at 3-min intervals (Fig. $5A_1$). In cells satisfying the criterion of stable baseline responses (<15% variation in 10 min), we subsequently perfused the cell with standard extracellular solution for 3 min to wash out ACh, applied 2 mM MTSEA for 2 min, washed out MTSEA for 5 min, and puffed 300 μM ACh to evoke I_{ACh} (Fig. $5A_2$). We compared I_{ACh} before and after MTSEA application to test whether MTSEA changed receptor function. Changes in agonist-induced currents indi-

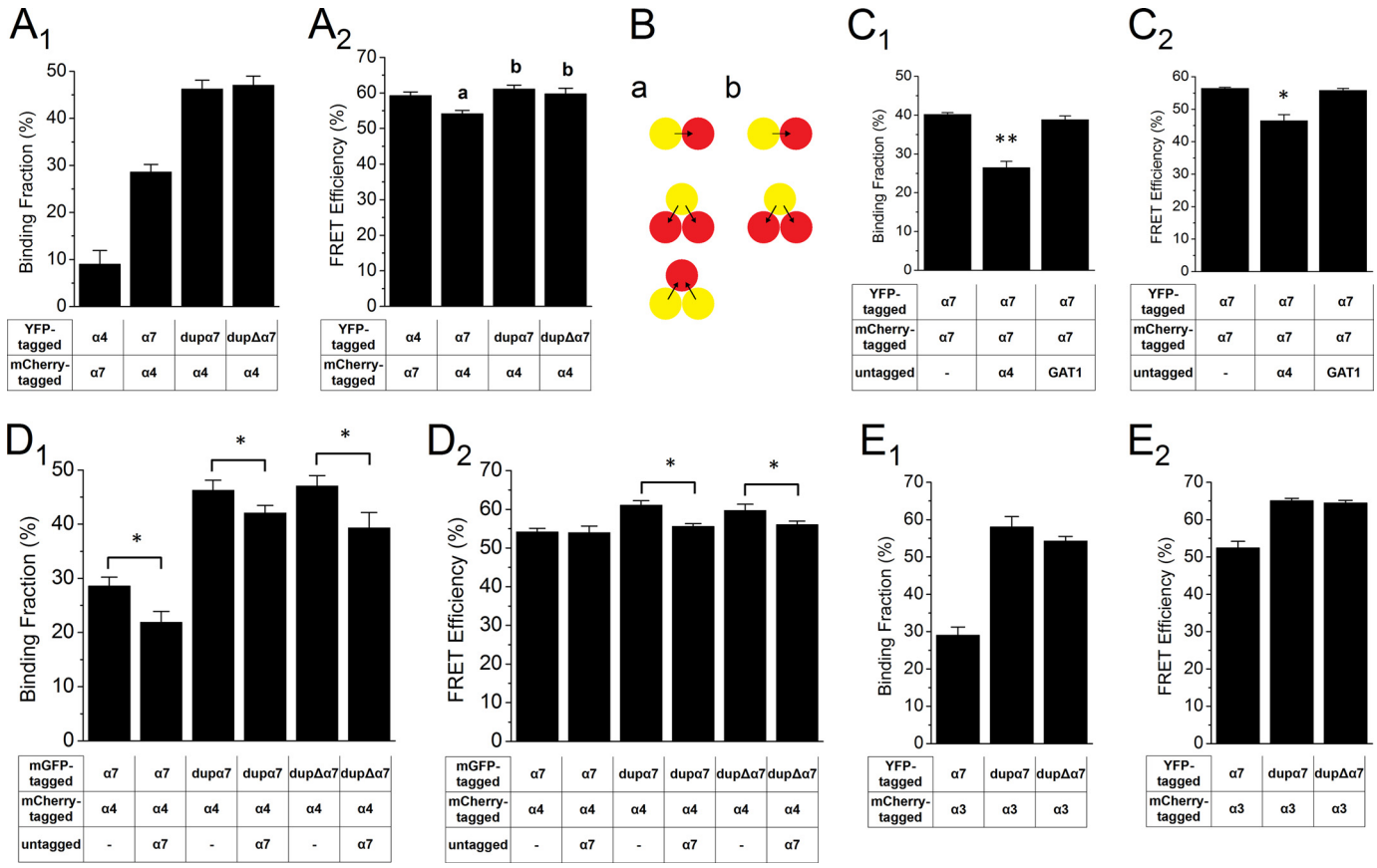

FIGURE 4. **FLIM revealed potential interaction of duplicated subunits with other nAChR subtypes.** A_1 and A_2, Neuro2a cells were transfected with indicated nAChR subunits and were imaged alive using FLIM. Binding fraction (A_1) and FRET efficiency (A_2) were calculated. α7, dupα7, and dupΔα7 interact with the human α4 subunit. *B,* schematic of FRET between donors and acceptors in a dimer or trimer. The *yellow circle* represents the donor (YFP molecule attached to a nAChR subunit), and the *red circle* represents the acceptor (YFP molecule attached to a nAChR subunit). An *arrow* represents energy transfer between the donor and the acceptor. C_1 and C_2, co-expression of untagged α4, but not GAT1, decreased the FRET between the α7-YFP/α7-mCherry pair. D_1 and D_2, co-expression of untagged full-length α7 subunit decreased the FRET between the α7-YFP/α4-mCherry, dupα7-YFP/α4-mCherry, and dupΔα7-YFP/α4-mCherry pairs. E_1 and E_2, α7, dupα7, and dupΔα7 interact with the human α3 subunit. *Error bars* are ± S.E., and $n = 20–30$ cells for each condition. **, $p < 0.01$; *, $p < 0.05$.

cate that the receptors include subunits with the cysteine mutation.

We transfected Neuro2a cells with α7 DNA constructs containing the C116S mutation. As a control, we transfected α7-mCherry, α7-mCherry + dupα7-GFP, or α7-mCherry + dupΔα7-GFP into Neuro2a cells and tested whether MTSEA changed receptor function. As expected, MTSEA did not change I_{ACh} in the transfected cells (Fig. 5, B_1, C_1, and D_1), confirming that introducing the C116S mutation was sufficient to prevent MTSEA from affecting the receptor's function. We next transfected α7-mCherry with both C116S and L9′C mutations into Neuro2a cells. In this situation, all of the subunits in the functional receptors are accessible to MTSEA. Indeed, we observed that MTSEA inhibited I_{ACh} by 54 ± 7% ($n = 5$, $p = 0.002$) (Fig. 5, B_2 and E_1). These results indicated that the assay was valid to reveal whether cysteine-containing subunits exist in functional receptors.

We next tested whether MTSEA changes receptor function in Neuro2a cells transfected with α7-mCherry containing the C116S mutation and either the dupα7-GFP or dupΔα7-GFP construct containing both C116S and L9′C mutations. We recorded I_{ACh} from cells showing both GFP and mCherry fluorescence and found that MTSEA, respectively, inhibited I_{ACh} by 63 ± 5% ($n = 7$, $p < 0.0001$) and by 43 ± 2% ($n = 6$, $p < 0.0001$) in cells expressing dupα7-GFP + α7-mCherry and dupΔα7-GFP + α7-mCherry (Fig. 5, C_2, D_2, and E_2). Note that the MTSEA effects on these cells were similar to those on cells expressing α7-L9′C subunits only. These results suggested that both dupα7 and dupΔα7 subunits were able to form functional receptors with α7 subunits, and in this expression system, most functional receptors had dupα7 or dupΔα7 subunits.

SCAM analysis suggests that in Neuro2a cells dupα7 or dupΔα7 subunits commonly assemble with α7 subunits forming functional receptors. To understand whether the presence of dupα7 or dupΔα7 subunits changes function of α7 receptors, we tested the dose-response relationship of I_{ACh} in Neuro2a cells transfected with α7 only, α7 + dupα7, or α7 + dupΔα7 subunits (Fig. 6, *A–C*). I_{ACh} in all transfected cells reached maximum levels when ACh exceeded 1 mM (Fig. 6*D*). The shifts of dose-response curves were not statistically significant (Fig. 6*D*). The Hill efficient was similar in α7 only (1.51 ± 0.25), α7 + dupα7 (1.48 ± 0.34), or dupΔα7 + α7 (1.60 ± 0.44), and the EC_{50} value was similar in α7 only (192 ± 21 μM), α7 + dupα7 (158 ± 24 μM,) and α7 + dupΔα7 cells (218 ± 31 μM), respectively. These data suggest that the presence of dupα7 and dupΔα7 does not alter the ACh sensitivity of α7 receptors.

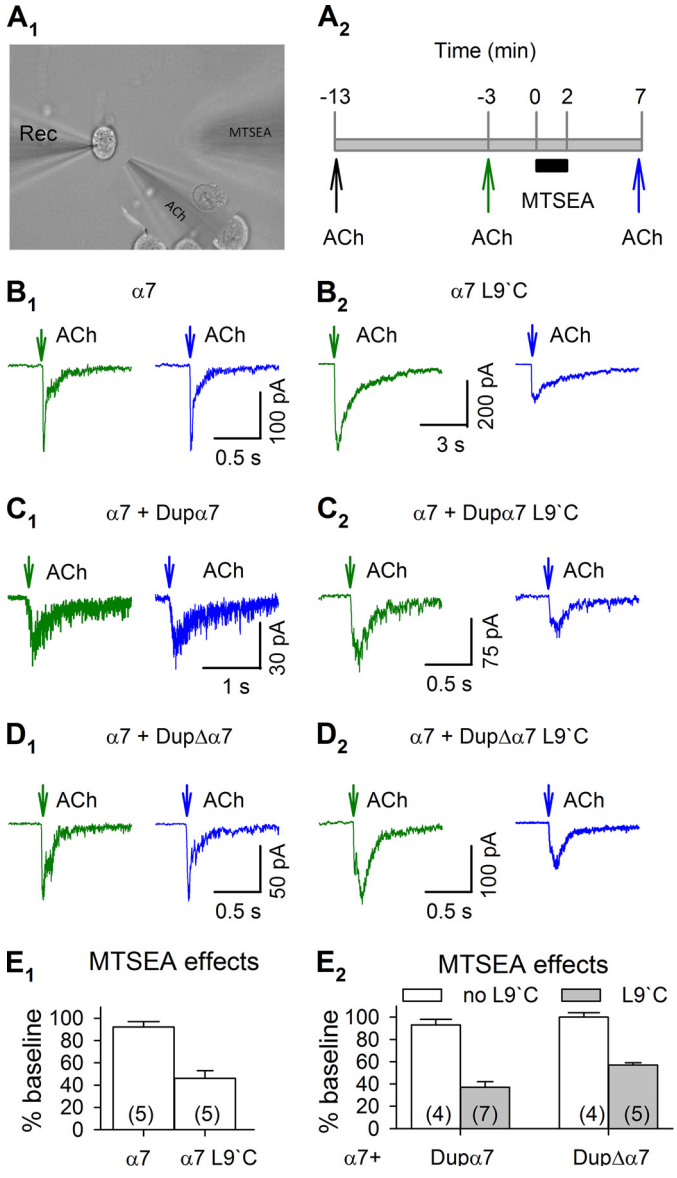

FIGURE 5. **SCAM evidence for the co-assembly of α7 and dupα7 or dupΔα7 subunits in functional nAChRs.** A_1, picture showing the whole-cell patch clamp recording from a Neuro2a cell, and the application of ACh and MTSEA. A_2, timeline of ACh and MTSEA application. MTSEA did not change α7 receptor function in cells expressing α7 subunit alone (B_1), α7 + dupα7 subunits (C_1), and α7 + dupΔα7 subunits (D_1). When the L9′C mutation was introduced into α7 subunits, MTSEA inhibited ACh-induced currents (B_2). When the L9′C mutation was introduced into dupα7 and dupΔα7, MTSEA attenuated ACh-induced currents in cells expressing α7 + dupα7 subunits (C_2) and α7 + dupΔα7 subunits (D_2). E_1 and E_2, summary of MTSEA effects on each group of cells. All subunits also included the C116S or aligning mutations. *Numbers in parentheses* indicate the number of cells examined.

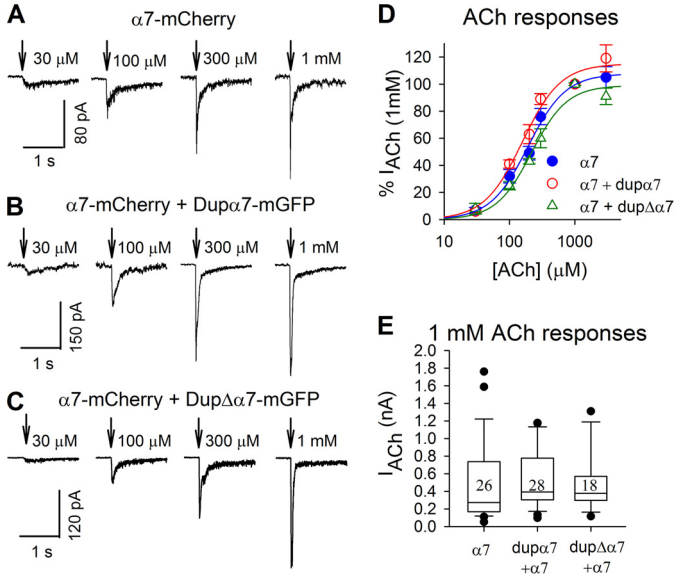

FIGURE 6. **dupα7 and dupΔα7 subunits did not change ACh responses of α7 receptors.** Responses to 30–3000 μM ACh were recorded from cells expressing α7 subunits (*A*), α7 + dupα7 subunits (*B*), and α7 + dupΔα7 subunits (*C*). The peaks of ACh currents were normalized to those of the 1 mM ACh-induced ones in individual cells, and the normalized currents were used to depict dose-response curves (*D*). Each point is averaged from 5–9 cells and is shown as mean ± S.E. The 1 mM ACh-induced currents are shown in box plots (*E*). *Numbers* in the box indicate the numbers of cells.

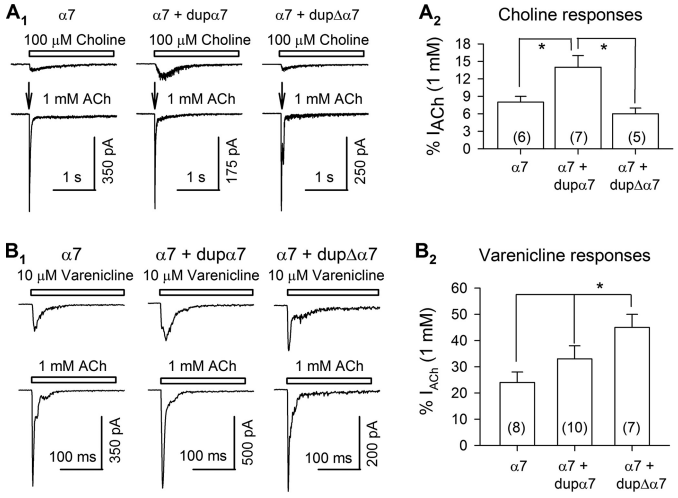

FIGURE 7. **Choline- and varenicline-evoked α7 currents.** Choline (100 μM) (A_1) and varenicline (10 μM) (B_1) induced inward currents in Neuro2a cells expressing α7 subunits, α7 + dupα7 subunits, and α7 + dupΔα7 subunits. In the same cells, 1 mM ACh-induced currents were also recorded (*lower panels* in A_1 and B_1). The responses of choline and varenicline were normalized to those of 1 mM ACh, and the normalized responses were illustrated in A_2 and B_2, respectively. *Numbers in parentheses* indicate the number of cells examined. *, $p < 0.05$.

Channel Properties of dupα7/α7 and dupΔα7/α7 Heteromers—We next tested whether dupα7 and dupΔα7 subunits affect the responses of α7 receptors to choline, another endogenous agonist, and to varenicline, a full agonist. We activated α7 receptors by puffing (20 p.s.i.) 100 μM choline or 10 μM varenicline (both are less than EC_{50}) (41, 42) (Fig. 7, A_1 and B_1, *upper panels*). On the same cell, we applied 1 mM ACh to evoke maximal activation of α7 receptors (Fig. 7, A_1 and B_1, *lower panels*). Then we normalized choline- and varenicline-induced currents to 1 mM ACh-evoked currents (Fig. 7, A_2 and B_2). This process reduced the variability introduced by differences in plasma membrane receptor numbers among individual cells, and by the process of deliberately selecting fluorescent cells. Choline induced a larger relative current in cells expressing dupα7 + α7 subunits (14 ± 2%, $n = 8$) than those expressing either α7 subunits alone (8 ± 1%, $n = 6$) or dupΔα7 + α7 subunits (6 ± 1%, $n = 7$) ($p = 0.01$, one-way analysis of variance) (Fig. 7A_2). Varenicline-induced currents were significantly larger in cells expressing dupΔα7 + α7 subunits (45 ± 5%, $n = 7$) than in those expressing α7 subunits alone (24 ± 4%, $n = 8$) or those expressing dupα7 + α7 subunits (33 ± 5%, $n = 10$) ($p = 0.02$,

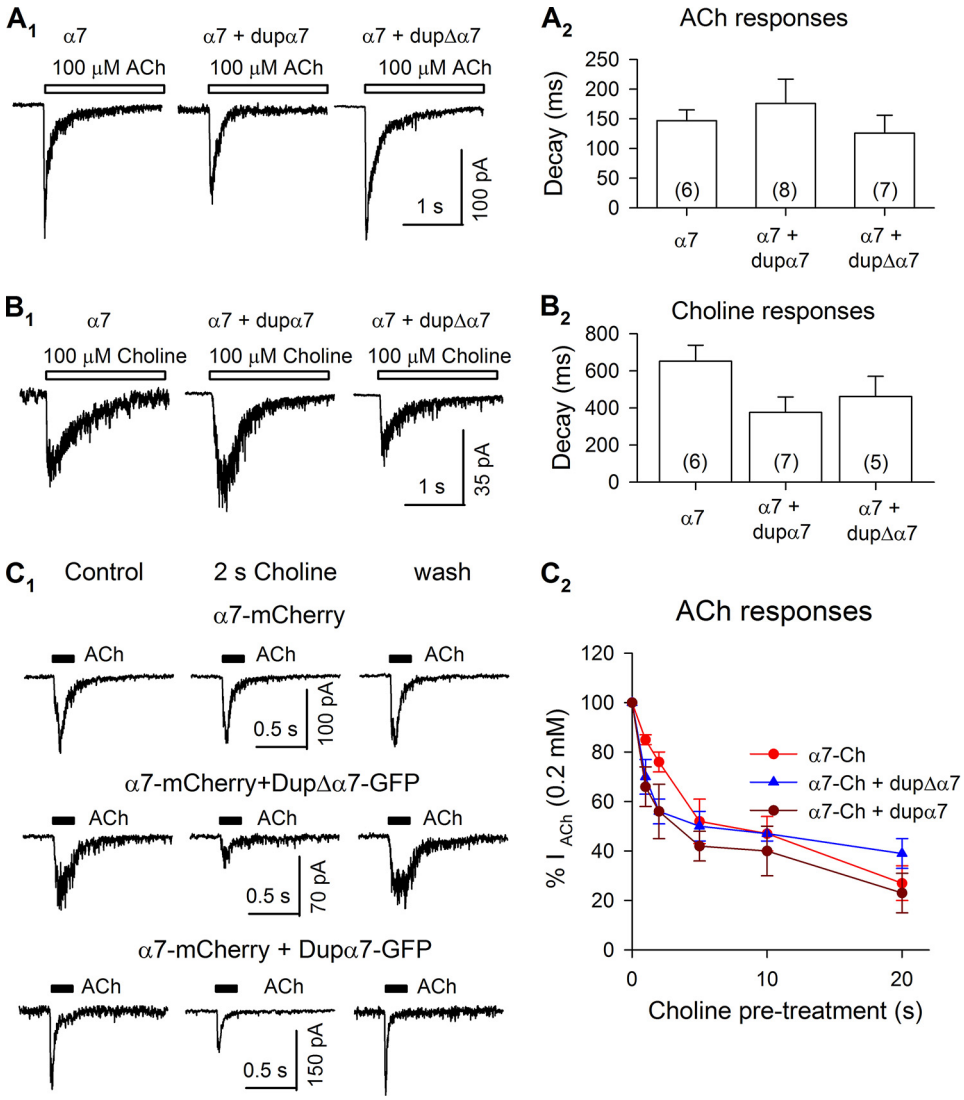

FIGURE 8. **Desensitization of α7 receptors.** 100 μM ACh (A_1) or 100 μM choline (B_1) was applied for 2 s to Neuro2a cells expressing α7 subunits, α7 + dupα7 subunits, and α7 + dupΔα7 subunits. The decay time constants of these responses were measured and summarized in A_2 and B_2. C_1, prolonged preincubation with 20 μM choline reversibly attenuated α7 receptor currents induced by 200 μM ACh. C_2, time course of desensitization by 20 μM choline. Each point in C_2 was averaged from 5 to 9 cells expressing α7 subunits only (*red circle*), α7 + dupΔα7 subunits (*blue triangle*), or α7 + dupα7 subunits (*brown circle*).

one-way analysis of variance) (Fig. 7B_2). These data suggest that the presence of dupα7 subunits may increase the sensitivity of α7 receptors to choline, but co-assembly of dupΔα7 with α7 subunits produced no significant change in sensitivity compared with homopentameric α7 receptors. However, the presence of dupΔα7 subunits may enhance the sensitivity of α7 receptors to varenicline.

Because 1 mM ACh evoked near-saturating currents, activating the great majority of α7 receptors (Fig. 6*D*), the size of 1 mM ACh-induced currents may correlate well with the number of functional receptors. We compared 1 mM ACh-induced currents in cells expressing α7 subunits alone, α7 + dupα7 subunits, and α7 + dupΔα7 subunits 72 h after transfection. As illustrated in Fig. 6*E*, the peak amplitude of I_{ACh} did not differ among groups of cells. These data suggest that dupα7 and dupΔα7 did not alter the number of α7 receptors. We acknowledge that ascertainment bias could have been introduced by the process of identifying and studying the fluorescent cells.

We applied 100 μM ACh and 100 μM choline for relatively prolonged pulses lasting 2 s, whereas we measured voltage-clamp currents (Fig. 8, A_1 and B_1). Such experiments represent the classical tests for desensitization kinetics of nAChRs. As shown in Fig. 8, A_2 and B_2, we found that the presence of dupα7 and dupΔα7 did not alter the desensitization kinetics of α7 receptors in the presence of ACh and choline. In all cases, desensitization was nearly complete during the pulse.

Endogenous choline levels are around 35 μM in the neonatal nervous system, and become ~3 times lower in the adult (43). It remains unknown whether the loss of function in a schizophrenia patient carrying dupΔα7 receptors comes from less activation by choline, accelerated desensitization, or more complete desensitization of α7 receptors in the presence of choline at circulating concentrations. To address these issues, we tested receptor activation by 20 μM choline, and we compared 200 μM ACh-induced currents before and after preincubation with 20 μM choline for 1–60 s (Fig. 8, C_1 and C_2). 20 μM choline induced

no detectable currents in all cells we recorded (data not shown). Preincubation with 20 μM choline up to 5 s reversibly attenuated ACh currents by ~50% in cells expressing α7 subunits alone, dupα7 + α7 subunits, and dupΔα7 + α7 subunits (Fig. 8, C_1 and C_2). The briefest preincubations with choline, 1 or 2 s, reversibly attenuated ACh-induced currents in cells expressing α7 subunits alone by 14 ± 3% (n = 6) and 24 ± 3% (n = 5), respectively. Interestingly, the attenuations were significantly greater in cells expressing α7 + dupα7 subunits (1-s choline by 34 ± 8%, n = 7; 2-s choline by 44 ± 11%, n = 5) and α7 + dupΔα7 subunits (1-s choline by 30 ± 7%, n = 5; 2-s choline by 44 ± 5%, n = 5) (Fig. 8C_2). These results support the hypothesis that the presence of dupα7 and dupΔα7 enhances some aspects of choline-induced desensitization at α7 receptors.

DISCUSSION

Exons 1–6 of *CHRNA7* correspond to the receptor's extracellular N-terminal region, which contains the ligand-binding domain. Exons 7 and 8 correspond to the first three transmembrane regions, M1, M2 and M3, and M2 constitutes the ion channel of the receptor (44). Exons 9 and 10 encode its intracellular cytoplasmic loop, the fourth transmembrane region, M4, and the extracellular C terminus. *CHRFAM7A*, containing only exons 5–10 of *CHRNA7*, lacks the signal peptide as well as part of the extracellular N-terminal region, including one of the three *N*-glycosylation sites. This lack of a ligand-binding domain renders it unsurprising that dupα7, when expressed alone in *Xenopus* oocytes or Neuro2a cells, fails to produce ACh-induced current. In addition, previous studies have demonstrated that the N-terminal extracellular domain of nAChR plays a leading role in mediating assembly and determines the specificity of the intersubunit recognition (45–47). This study confirms that in a heterologous expression system, a truncated nAChR subunit lacking both signal peptide and part of the N-terminal extracellular domain is 1) processed in a similar way as the full-length subunit; 2) assembled with the full-length subunit; 3) trafficked to the cell membrane; and 4) incorporated into a functional channel.

Although the N-terminal extracellular domain is important for the initial association between subunits, a downstream domain, the cytoplasmic loop between M1 and M2, participates in the subsequent interaction and stabilization of the oligomeric complex (48). Further downstream, the M3-M4 intracellular loop also affects nAChR assembly (49, 50). Assembly of dupα7 and dupΔα7 with full-length α7 suggests that other regions of sequence may mediate the interaction between subunits and thus compensate for the lack of the N terminus.

The duplicated subunits also interact with other nAChR subtypes, such as α4 and α3, suggesting that they may have broad effects on nAChR function, depending on the cell types and brain regions in which they are expressed. Because the N-terminal extracellular domain controls specificity of subunit interaction, future studies should examine whether duplicated subunits assemble with other Cys loop receptors, such as serotonin 5-HT_3, that do not normally interact with full-length α7. We do not know whether the interactions of the duplicated α7 subunit, found here in the admittedly forced heterologous system, also occur in human neurons.

Immunostaining of dupα7 overexpressed in SH-EP cells confirmed that translated peptide contains the sequence for the α7 subunit (19). The translation of *CHRFAM7AΔ2bp*, however, is based only on prediction. When the 2-bp deletion in exon 6 is present, translation is likely to start at one of the two initiating methionines in exon 6. The peptide is out of frame for either 6 or 13 amino acids, depending on which ATG is used, until the 2-bp deletion is reached. At that point, the amino acid sequence returns to the reading frame of the α7 subunit. The resulting protein, dupΔα7, is smaller than dupα7 and lacks a larger portion of the agonist-binding domain. We fused a fluorescent protein into the M3-M4 loop of dupΔα7 and expressed the labeled protein in Neuro2a cells. Fluorescent signals were observed, and they overlap with the signals from fluorescently labeled full-length α7. Our confocal imaging data confirmed that dupΔα7 is indeed translated, and the protein is in-frame with α7.

We have studied the effect of the duplicated α7 genes on α7 nAChR function. In theory, they could regulate receptor expression and function in other ways, such as at the RNA level. Furthermore, several ATGs in *CHRFAM7A* could result in truncated transcripts that do not contain *CHRNA7* coding sequence. Because of the frameshift in *CHRFAM7AΔ2bp*, use of the dupα7 subunit initiating methionine would encode a unique 40-amino acid peptide, terminated by a stop codon. With no homology to α7, it is unlikely that such a truncated peptide would assemble with α7 subunits.

The duplicated subunits may have a role in inflammatory responses. Recent studies described α7 nAChR as a link in the cholinergic anti-inflammatory pathway and an anti-inflammatory target (51–53). dupα7 is highly expressed in macrophages, and it is down-regulated at the mRNA level by IL-1, LPS, and nicotine (20, 54). Duplicated subunits could therefore modulate α7 receptor-mediated cholinergic anti-inflammatory responses. We noted that co-expression of α7 increased the proportion of dupα7-expressing cells by 2-fold (data not shown); we do not know whether this occurred because α7 enhances dupα7 mRNA expression or acts as a protein chaperone for dupα7 survival. Thus, investigating dupα7/α7 pathways may have medical applications in the treatment of inflammatory disorders.

We found that co-expression of either duplicated subunit with α7 subunits in mammalian cells had no marked effects on ACh-induced currents. This finding contrasts with previous studies in oocytes, showing a dominant negative effect of dupα7 on the full-length receptor (19, 20). Many previous studies show that ion channels and receptors assemble differently in these two expression systems, probably in several ways. First, dupα7 and dupΔα7 genes and proteins are expressed at extremely low levels in mammalian cells. Although we used equimolar amounts of α7 and dupα7 DNA for transfection, the actual mRNA and protein ratio of dupα7/α7 was probably 1:10 or lower. Because small amounts of dupα7 subunits were present, few α7/dupα7 heteromers included more than one dupα7 subunit. A previous study shows that nAChRs containing only a single non-α7 subunit, and therefore lacking two α7-α7 interfaces, do function rather well (55); but an additional non-α7 subunit does abolish function (55). This surfeit of dupα7 or

dupΔα7 subunits may be possible in oocytes, producing the apparent dominant negative effect, but apparently not in the present mammalian system. Second, our studies in Neuro2a cells also included RIC-3 (resistant to inhibitor of cholinesterase) expression. RIC-3 is an endoplasmic reticulum chaperone for nAChRs (56–58). The effects of the RIC-3 level on α7 receptors display an inverted U-shape dose-response relation (57). RIC-3 also shows differential effects when co-expressed with various ligand-gated ion channels as follows: enhancing functional expression of multiple nAChR subtypes and inhibiting 5-HT_3 receptors and several nAChR subtypes, including α3β4, but had no effect on either GABA or glutamate receptors (59–61). We co-expressed RIC-3 in Neuro2a cells for all our electrophysiological experiments to enable functional expression of α7 on the cell membrane. However, we do not know what influence RIC-3 may have on duplicated subunits and how RIC-3 may regulate the effect of duplicated subunits on full-length α7 receptors.

Although we did not observe a significant difference in the ACh response of α7 receptors when dupα7 or dupΔα7 was co-expressed, dupΔα7/α7 did display a lower choline sensitivity than dupα7/α7 heteromers. In addition, dupα7/α7 or dupΔα7/α7 receptors desensitize more quickly during brief (1 to 2 s) exposure to physiological concentrations of choline. Genetic and neurobiological studies suggest that choline availability may contribute to the development of schizophrenia-associated sensory gating deficits (62), and perinatal dietary choline supplementation has been tested for lowering schizophrenia risk, with positive results (63). The copy of the duplicated gene with the 2-bp deletion, *CHRFAM7AΔ2bp*, is found much more frequently in schizophrenic patients than in control subjects with no mental illness (16) and is associated with abnormal sensory processing (64). Our electrophysiological data, suggesting that dupΔα7 lacks the augmentation of choline sensitivity produced by dupα7, may be relevant to a decreased efficacy of choline during development in subjects that carry this 2-bp deletion.

Varenicline produces improved cognitive performance in schizophrenic patients (65–67). The underlying mechanisms remain unclear because varenicline activates at least three types of nAChRs. It is a partial agonist for α4β2 (EC_{50} = 2.3 μM, with maximal efficacy of 13% relative to ACh) and α3β4 (EC_{50} = 55 μM with maximal efficacy of 75% relative to ACh) nAChRs but a full agonist for α7 nAChRs (EC_{50} = 18 μM) (42). We observed a moderately enhanced sensitivity of α7/dupΔα7 nAChRs relative to α7 and α7/dupα7 receptors, supporting the present concepts that α7 nAChRs are promising targets for development of drugs to treat cognitive impairment in schizophrenia.

Acknowledgments—We thank Sheri McKinney for providing neuron cultures. We also thank Drs. Christopher I. Richards and Bruce N. Cohen for helpful discussions.

REFERENCES

1. Gershon, E. S. (2000) Bipolar illness and schizophrenia as oligogenic diseases: implications for the future. *Biol. Psychiatry* **47,** 240–244
2. Freedman, R., Leonard, S., Olincy, A., Kaufmann, C. A., Malaspina, D., Cloninger, C. R., Svrakic, D., Faraone, S. V., and Tsuang, M. T. (2001) Evidence for the multigenic inheritance of schizophrenia. *Am. J. Med. Genet.* **105,** 794–800
3. Freedman, R., Adams, C. E., and Leonard, S. (2000) The α7-nicotinic acetylcholine receptor and the pathology of hippocampal interneurons in schizophrenia. *J. Chem. Neuroanat.* **20,** 299–306
4. Guan, Z. Z., Zhang, X., Blennow, K., and Nordberg, A. (1999) Decreased protein level of nicotinic receptor α7 subunit in the frontal cortex from schizophrenic brain. *Neuroreport.* **10,** 1779–1782
5. Court, J., Spurden, D., Lloyd, S., McKeith, I., Ballard, C., Cairns, N., Kerwin, R., Perry, R., and Perry, E. (1999) Neuronal nicotinic receptors in dementia with Lewy bodies and schizophrenia: α-bungarotoxin and nicotine binding in the thalamus. *J. Neurochem.* **73,** 1590–1597
6. Marutle, A., Zhang, X., Court, J., Piggott, M., Johnson, M., Perry, R., Perry, E., and Nordberg, A. (2001) Laminar distribution of nicotinic receptor subtypes in cortical regions in schizophrenia. *J. Chem. Neuroanat.* **22,** 115–126
7. Freedman, R., Coon, H., Myles-Worsley, M., Orr-Urtreger, A., Olincy, A., Davis, A., Polymeropoulos, M., Holik, J., Hopkins, J., Hoff, M., Rosenthal, J., Waldo, M. C., Reimherr, F., Wender, P., Yaw, J., Young, D. A., Breese, C. R., Adams, C., Patterson, D., Adler, L. E., Kruglyak, L., Leonard, S., and Byerley, W. (1997) Linkage of a neurophysiological deficit in schizophrenia to a chromosome 15 locus. *Proc. Natl. Acad. Sci. U.S.A.* **94,** 587–592
8. Leonard, S., and Freedman, R. (2006) Genetics of chromosome 15q13-q14 in schizophrenia. *Biol. Psychiatry* **60,** 115–122
9. Stephens, S. H., Logel, J., Barton, A., Franks, A., Schultz, J., Short, M., Dickenson, J., James, B., Fingerlin, T. E., Wagner, B., Hodgkinson, C., Graw, S., Ross, R. G., Freedman, R., and Leonard, S. (2009) Association of the 5′-upstream regulatory region of the α7 nicotinic acetylcholine receptor subunit gene (CHRNA7) with schizophrenia. *Schizophr. Res.* **109,** 102–112
10. Leonard, S., Gault, J., Hopkins, J., Logel, J., Vianzon, R., Short, M., Drebing, C., Berger, R., Venn, D., Sirota, P., Zerbe, G., Olincy, A., Ross, R. G., Adler, L. E., and Freedman, R. (2002) Association of promoter variants in the α7 nicotinic acetylcholine receptor subunit gene with an inhibitory deficit found in schizophrenia. *Arch. Gen. Psychiatry* **59,** 1085–1096
11. Gault, J., Robinson, M., Berger, R., Drebing, C., Logel, J., Hopkins, J., Moore, T., Jacobs, S., Meriwether, J., Choi, M. J., Kim, E. J., Walton, K., Buiting, K., Davis, A., Breese, C., Freedman, R., and Leonard, S. (1998) Genomic organization and partial duplication of the human α7 neuronal nicotinic acetylcholine receptor gene (CHRNA7). *Genomics* **52,** 173–185
12. Riley, B., Williamson, M., Collier, D., Wilkie, H., and Makoff, A. (2002) A 3-Mb map of a large segmental duplication overlapping the α7-nicotinic acetylcholine receptor gene (CHRNA7) at human 15q13-q14. *Genomics* **79,** 197–209
13. Locke, D. P., Archidiacono, N., Misceo, D., Cardone, M. F., Deschamps, S., Roe, B., Rocchi, M., and Eichler, E. E. (2003) Refinement of a chimpanzee pericentric inversion breakpoint to a segmental duplication cluster. *Genome Biol.* **4,** R50
14. Gault, J., Hopkins, J., Berger, R., Drebing, C., Logel, J., Walton, C., Short, M., Vianzon, R., Olincy, A., Ross, R. G., Adler, L. E., Freedman, R., and Leonard, S. (2003) Comparison of polymorphisms in the α7 nicotinic receptor gene and its partial duplication in schizophrenic and control subjects. *Am. J. Med. Genet. B Neuropsychiatr. Genet.* **123B,** 39–49
15. Flomen, R. H., Davies, A. F., Di Forti, M., La Cascia, C., Mackie-Ogilvie, C., Murray, R., and Makoff, A. J. (2008) The copy number variant involving part of the α7 nicotinic receptor gene contains a polymorphic inversion. *Eur. J. Hum. Genet.* **16,** 1364–1371
16. Sinkus, M. L., Lee, M. J., Gault, J., Logel, J., Short, M., Freedman, R., Christian, S. L., Lyon, J., and Leonard, S. (2009) A 2-base pair deletion polymorphism in the partial duplication of the α7 nicotinic acetylcholine gene (CHRFAM7A) on chromosome 15q14 is associated with schizophrenia. *Brain Res.* **1291,** 1–11
17. Flomen, R. H., Collier, D. A., Osborne, S., Munro, J., Breen, G., St Clair, D., and Makoff, A. J. (2006) Association study of CHRFAM7A copy number and 2-bp deletion polymorphisms with schizophrenia and bipolar affective disorder. *Am. J. Med. Genet. B Neuropsychiatr. Genet.* **141B,** 571–575
18. Villiger, Y., Szanto, I., Jaconi, S., Blanchet, C., Buisson, B., Krause, K. H., Bertrand, D., and Romand, J. A. (2002) Expression of an α7 duplicate

nicotinic acetylcholine receptor-related protein in human leukocytes. *J. Neuroimmunol.* **126,** 86–98
19. Araud, T., Graw, S., Berger, R., Lee, M., Neveu, E., Bertrand, D., and Leonard, S. (2011) The chimeric gene CHRFAM7A, a partial duplication of the CHRNA7 gene, is a dominant negative regulator of α7* nAChR function. *Biochem. Pharmacol.* **82,** 904–914
20. de Lucas-Cerrillo, A. M., Maldifassi, M. C., Arnalich, F., Renart, J., Atienza, G., Serantes, R., Cruces, J., Sánchez-Pacheco, A., Andrés-Mateos, E., and Montiel, C. (2011) Function of partially duplicated human α77 nicotinic receptor subunit CHRFAM7A gene: potential implications for the cholinergic anti-inflammatory response. *J. Biol. Chem.* **286,** 594–606
21. Drenan, R. M., Nashmi, R., Imoukhuede, P., Just, H., McKinney, S., and Lester, H. A. (2008) Subcellular trafficking, pentameric assembly and subunit stoichiometry of neuronal nicotinic ACh receptors containing fluorescently-labeled α6 and β3 subunits. *Mol. Pharmacol.* **73,** 27–41
22. Murray, T. A., Liu, Q., Whiteaker, P., Wu, J., and Lukas, R. J. (2009) Nicotinic acetylcholine receptor α7 subunits with a C2 cytoplasmic loop yellow fluorescent protein insertion form functional receptors. *Acta Pharmacol. Sin.* **30,** 828–841
23. Srinivasan, R., Richards, C. I., Xiao, C., Rhee, D., Pantoja, R., Dougherty, D. A., Miwa, J. M., and Lester, H. A. (2012) Pharmacological chaperoning of nicotinic acetylcholine receptors reduces the endoplasmic reticulum stress response. *Mol. Pharmacol.* **81,** 759–769
24. Slimko, E. M., McKinney, S., Anderson, D. J., Davidson, N., and Lester, H. A. (2002) Selective electrical silencing of mammalian neurons *in vitro* by the use of invertebrate ligand-gated chloride channels. *J. Neurosci.* **22,** 7373–7379
25. King, C., Sarabipour, S., Byrne, P., Leahy, D. J., and Hristova, K. (2014) The FRET signatures of noninteracting proteins in membranes: simulations and experiments. *Biophys. J.* **106,** 1309–1317
26. Richards, C. I., Luong, K., Srinivasan, R., Turner, S. W., Dougherty, D. A., Korlach, J., and Lester, H. A. (2012) Live-cell imaging of single receptor composition using zero-mode waveguide nanostructures. *Nano Lett.* **12,** 3690–3694
27. Simonson, P. D., Deberg, H. A., Ge, P., Alexander, J. K., Jeyifous, O., Green, W. N., and Selvin, P. R. (2010) Counting bungarotoxin binding sites of nicotinic acetylcholine receptors in mammalian cells with high signal/noise ratios. *Biophys. J.* **99,** L81–L83
28. Srinivasan, R., Pantoja, R., Moss, F. J., Mackey, E. D., Son, C. D., Miwa, J., and Lester, H. A. (2011) Nicotine upregulates α4β2 nicotinic receptors and ER exit sites via stoichiometry-dependent chaperoning. *J. Gen. Physiol.* **137,** 59–79
29. Xiao, C., Nashmi, R., McKinney, S., Cai, H., McIntosh, J. M., and Lester, H. A. (2009) Chronic nicotine selectively enhances α4β2* nicotinic acetylcholine receptors in the nigrostriatal dopamine pathway. *J. Neurosci.* **29,** 12428–12439
30. Zoli, M., Moretti, M., Zanardi, A., McIntosh, J. M., Clementi, F., and Gotti, C. (2002) Identification of the nicotinic receptor subtypes expressed on dopaminergic terminals in the rat striatum. *J. Neurosci.* **22,** 8785–8789
31. Moss, F. J., Imoukhuede, P. I., Scott, K., Hu, J., Jankowsky, J. L., Quick, M. W., and Lester, H. A. (2009) GABA transporter function, oligomerization state, and anchoring: correlates with subcellularly resolved FRET. *J. Gen. Physiol.* **134,** 489–521
32. Srinivasan, R., Richards, C. I., Dilworth, C., Moss, F. J., Dougherty, D. A., and Lester, H. A. (2012) Forster resonance energy transfer (FRET) correlates of altered subunit stoichiometry in Cys loop receptors, exemplified by nicotinic α4β2. *Int. J. Mol. Sci.* **13,** 10022–10040
33. Miles, T. F., Dougherty, D. A., and Lester, H. A. (2013) The 5-HT_3AB receptor shows an A_3B_2 stoichiometry at the plasma membrane. *Biophys. J.* **105,** 887–898
34. Nashmi, R., Dickinson, M. E., McKinney, S., Jareb, M., Labarca, C., Fraser, S. E., and Lester, H. A. (2003) Assembly of α4β2 nicotinic acetylcholine receptors assessed with functional fluorescently labeled subunits: effects of localization, trafficking, and nicotine-induced upregulation in clonal mammalian cells and in cultured midbrain neurons. *J. Neurosci.* **23,** 11554–11567
35. Bastiaens, P. I., and Squire, A. (1999) Fluorescence lifetime imaging microscopy: spatial resolution of biochemical processes in the cell. *Trends Cell Biol.* **9,** 48–52
36. Festy, F., Ameer-Beg, S. M., Ng, T., and Suhling, K. (2007) Imaging proteins *in vivo* using fluorescence lifetime microscopy. *Mol. BioSyst.* **3,** 381–391
37. Akabas, M. H., Kaufmann, C., Archdeacon, P., and Karlin, A. (1994) Identification of acetylcholine receptor channel-lining residues in the entire M2 segment of the α subunit. *Neuron* **13,** 919–927
38. Akabas, M. H., Stauffer, D. A., Xu, M., and Karlin, A. (1992) Acetylcholine receptor channel structure probed in cysteine-substitution mutants. *Science* **258,** 307–310
39. Papke, R. L., Stokes, C., Williams, D. K., Wang, J., and Horenstein, N. A. (2011) Cysteine accessibility analysis of the human α7 nicotinic acetylcholine receptor ligand-binding domain identifies L119 as a gatekeeper. *Neuropharmacology* **60,** 159–171
40. Xiao, C., Srinivasan, R., Drenan, R. M., Mackey, E. D., McIntosh, J. M., and Lester, H. A. (2011) Characterizing functional α6β2 nicotinic acetylcholine receptors *in vitro*: mutant β2 subunits improve membrane expression, and fluorescent proteins reveal responsive cells. *Biochem. Pharmacol.* **82,** 852–861
41. Zhao, L., Kuo, Y. P., George, A. A., Peng, J. H., Purandare, M. S., Schroeder, K. M., Lukas, R. J., and Wu, J. (2003) Functional properties of homomeric, human α7-nicotinic acetylcholine receptors heterologously expressed in the SH-EP1 human epithelial cell line. *J. Pharmacol. Exp. Ther.* **305,** 1132–1141
42. Mihalak, K. B., Carroll, F. I., and Luetje, C. W. (2006) Varenicline is a partial agonist at α4β2 and a full agonist at α7 neuronal nicotinic receptors. *Mol. Pharmacol.* **70,** 801–805
43. Miwa, J. M., Freedman, R., and Lester, H. A. (2011) Neural systems governed by nicotinic acetylcholine receptors: emerging hypotheses. *Neuron* **70,** 20–33
44. Changeux, J. P., Bertrand, D., Corringer, P. J., Dehaene, S., Edelstein, S., Léna, C., Le Novère, N., Marubio, L., Picciotto, M., and Zoli, M. (1998) Brain nicotinic receptors: structure and regulation, role in learning and reinforcement. *Brain Res. Brain Res. Rev.* **26,** 198–216
45. Yu, X.-M., and Hall, Z. W. (1991) Extracellular domains mediating ϵ subunit interactions of muscle acetylcholine receptor. *Nature* **352,** 64–67
46. Sumikawa, K., and Nishizaki, T. (1994) The amino acid residues 1–128 in the α subunit of the nicotinic acetylcholine receptor contain assembly signals. *Brain Res. Mol. Brain Res.* **25,** 257–264
47. Castillo, M., Mulet, J., Aldea, M., Gerber, S., Sala, S., Sala, F., and Criado, M. (2009) Role of the N-terminal α-helix in biogenesis of α7 nicotinic receptors. *J. Neurochem.* **108,** 1399–1409
48. García-Guzmán, M., Sala, F., Sala, S., Campos-Caro, A., and Criado, M. (1994) Role of two acetylcholine receptor subunit domains in homomer formation and intersubunit recognition, as revealed by α3 and α7 subunit chimeras. *Biochemistry* **33,** 15198–15203
49. Mukherjee, J., Kuryatov, A., Moss, S. J., Lindstrom, J. M., and Anand, R. (2009) Mutations of cytosolic loop residues impair assembly and maturation of α7 nicotinic acetylcholine receptors. *J. Neurochem.* **110,** 1885–1894
50. Kracun, S., Harkness, P. C., Gibb, A. J., and Millar, N. S. (2008) Influence of the M3-M4 intracellular domain upon nicotinic acetylcholine receptor assembly, targeting and function. *Br. J. Pharmacol.* **153,** 1474–1484
51. Libert, C. (2003) Inflammation: A nervous connection. *Nature* **421,** 328–329
52. Tracey, K. J. (2002) The inflammatory reflex. *Nature* **420,** 853–859
53. Ulloa, L. (2005) The vagus nerve and the nicotinic anti-inflammatory pathway. *Nat. Rev. Drug Discov.* **4,** 673–684
54. Benfante, R., Antonini, R. A., De Pizzol, M., Gotti, C., Clementi, F., Locati, M., and Fornasari, D. (2011) Expression of the α7 nAChR subunit duplicate form (CHRFAM7A) is down-regulated in the monocytic cell line THP-1 on treatment with LPS. *J. Neuroimmunol.* **230,** 74–84
55. Murray, T. A., Bertrand, D., Papke, R. L., George, A. A., Pantoja, R., Srinivasan, R., Liu, Q., Wu, J., Whiteaker, P., Lester, H. A., and Lukas, R. J. (2012) α7β2 nicotinic acetylcholine receptors assemble, function, and are activated primarily via their α7-α7 interfaces. *Mol. Pharmacol.* **81,** 175–188
56. Halevi, S., McKay, J., Palfreyman, M., Yassin, L., Eshel, M., Jorgensen, E.,

and Treinin, M. (2002) The *C. elegans* ric-3 gene is required for maturation of nicotinic acetylcholine receptors. *EMBO J.* **21,** 1012–1020
57. Alexander, J. K., Sagher, D., Krivoshein, A. V., Criado, M., Jefford, G., and Green, W. N. (2010) Ric-3 promotes α7 nicotinic receptor assembly and trafficking through the ER subcompartment of dendrites. *J. Neurosci.* **30,** 10112–10126
58. Wang, Y., Yao, Y., Tang, X. Q., and Wang, Z. Z. (2009) Mouse RIC-3, an endoplasmic reticulum chaperone, promotes assembly of the α7 acetylcholine receptor through a cytoplasmic coiled-coil domain. *J. Neurosci.* **29,** 12625–12635
59. Lansdell, S. J., Gee, V. J., Harkness, P. C., Doward, A. I., Baker, E. R., Gibb, A. J., and Millar, N. S. (2005) RIC-3 enhances functional expression of multiple nicotinic acetylcholine receptor subtypes in mammalian cells. *Mol. Pharmacol.* **68,** 1431–1438
60. Millar, N. S. (2008) RIC-3: a nicotinic acetylcholine receptor chaperone. *Br. J. Pharmacol.* **153,** S177–S183
61. Castillo, M., Mulet, J., Gutiérrez, L. M., Ortiz, J. A., Castelán, F., Gerber, S., Sala, S., Sala, F., and Criado, M. (2005) A dual role of the RIC-3 protein in trafficking of serotonin and nicotinic acetylcholine receptors. *J. Biol. Chem.* **280,** 27062–27068
62. Ross, R. G., Stevens, K. E., Proctor, W. R., Leonard, S., Kisley, M. A., Hunter, S. K., Freedman, R., and Adams, C. E. (2010) Research review: Cholinergic mechanisms, early brain development, and risk for schizophrenia. *J. Child Psychol. Psychiatry* **51,** 535–549
63. Ross, R. G., Hunter, S. K., McCarthy, L., Beuler, J., Hutchison, A. K., Wagner, B. D., Leonard, S., Stevens, K. E., and Freedman, R. (2013) Perinatal choline effects on neonatal pathophysiology related to later schizophrenia risk. *Am. J. Psychiatry* **170,** 290–298
64. Raux, G., Bonnet-Brilhault, F., Louchart, S., Houy, E., Gantier, R., Levillain, D., Allio, G., Haouzir, S., Petit, M., Martinez, M., Frebourg, T., Thibaut, F., and Campion, D. (2002) The 2-bp deletion in exon 6 of the "*α7-like*" nicotinic receptor subunit gene is a risk factor for the P50 sensory gating deficit. *Mol. Psychiatry* **7,** 1006–1011
65. Hong, L. E., Thaker, G. K., McMahon, R. P., Summerfelt, A., Rachbeisel, J., Fuller, R. L., Wonodi, I., Buchanan, R. W., Myers, C., Heishman, S. J., Yang, J., and Nye, A. (2011) Effects of moderate-dose treatment with varenicline on neurobiological and cognitive biomarkers in smokers and nonsmokers with schizophrenia or schizoaffective disorder. *Arch. Gen. Psychiatry* **68,** 1195–1206
66. Shim, J. C., Jung, D. U., Jung, S. S., Seo, Y. S., Cho, D. M., Lee, J. H., Lee, S. W., Kong, B. G., Kang, J. W., Oh, M. K., Kim, S. D., McMahon, R. P., and Kelly, D. L. (2012) Adjunctive varenicline treatment with antipsychotic medications for cognitive impairments in people with schizophrenia: a randomized double-blind placebo-controlled trial. *Neuropsychopharmacology* **37,** 660–668
67. Wing, V. C., Wass, C. E., Bacher, I., Rabin, R. A., and George, T. P. (2013) Varenicline modulates spatial working memory deficits in smokers with schizophrenia. *Schizophr. Res.* **149,** 190–191